Simulation results for fast ejectile and heavy-ion detectors

A SiNuRSE deliverable

Masoud Mahjour-Shafiei

1 September 2013

Contents

1 Introduction

In this report, the results of the simulations for heavy-ion, slow and fast ejectile detectors are presented. In particular, the methods were applied to the detection system of the experiment E105 which was performed in the autumn of 2012 at Experimental Storage Ring (ESR) in GSI [1]. This simulation contains the whole geometry including two DSSDs, two SiLi detectors, an object with two slits, a shield, two quadrupols, and finally a set of six pin diodes installed after the quadrupols. The simulations of the magnetic elements was performed by implementation of the magnetic transfer matrices in Geant4 [2]. The simulation, without magnetic elements, was implemented within the FairROOT framework [3], as well.

In order to perform a fair simulation, a dedicated event generator was developed to generate the decay fragments on-the-fly. For this particular simulation, such a generator was needed to study the decay of $^{58/56}$Ni* (ISGMR and ISGDR) into heavy and light fragments. However, the generator was developed to be capable of generating any type of fragments from any excited nucleus.

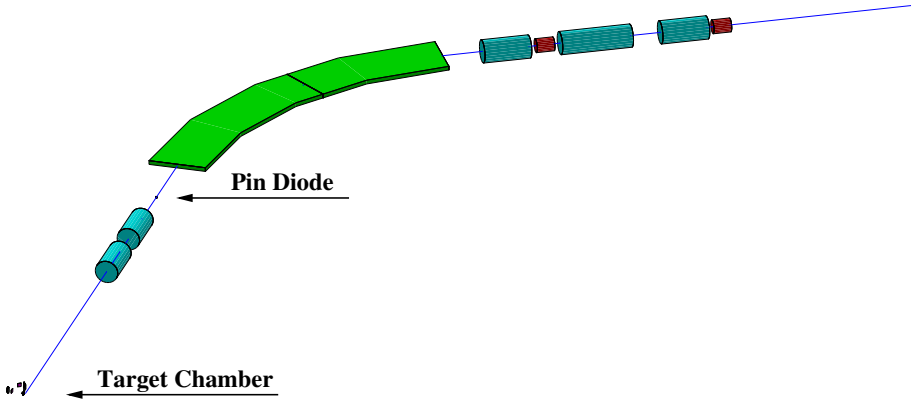

Figure 1: Part of ESR ring, objects shown in cyan, green, and red are quadrupoles, dipoles and sextupoles, respectively. The blue ray going through the objects is the reference ion trajectory.

2 Geometry description

In figure 1, part of ESR including the E105 setup is shown. In this figure the blue ray is the reference ion trajectory. Since the objects shown in this figure are all scaled down with the same factor, the pin diode (located between the first quadrupole doublets and the dipoles) is hardy visible. In order to implement the effect of the magnetic elements in the simulation instead of using the magnetic map of each element which would be CPU time consuming the transfer matrices were used [4]. Figure 2 shows part of the ESR ring which is used for E105 experiment. The blue rays in this figure are the beam-like heavy ions scattered from the gas jet target. The gas jet target is capable of injecting H and ^{4}He perpendicular to the circulating beam. The target-like light ejectiles are detected by the DSSDs, and the beam-like heavy ions and heavy fragments are detected by the pin diodes installed downstream.

The target chamber with its all components are shown in details in figure 3. A schematic drawing of the target chamber is also shown in figure 4. In the following subsections the target-chamber components and the pin diode which is installed outside the chamber are discussed in more details.

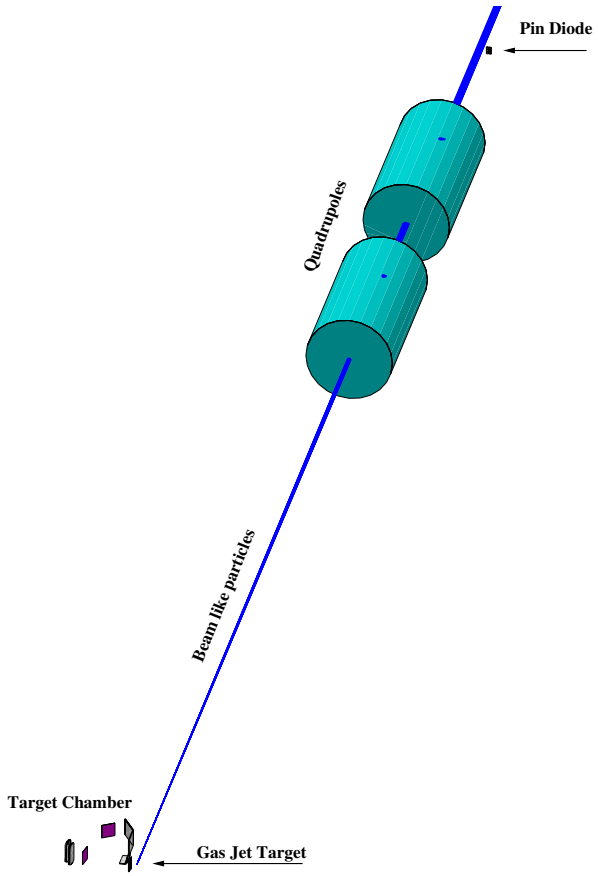

Figure 2: Schematics of part of ESR and the E105 setup including the target chamber components on the outer side of the ring and the pin diode on the inner side. The blue rays are beam-like heavy ions scattered from the gas jet target.

2.1 DSSDs

The target chamber contains two Double-sided Strip Silicon Detectors (DSSD). Each DSSD has an active area of 64×64 mm^2 and 128 strips with a thickness of 0.285 mm. First DSSD (hereafter DSSD#1) is positioned at 80.5° with respect to the beam axis and 251 mm away from the Interaction Region (IR). This DSSD covers up to 89° in laboratory frame which makes it desirable for probing elastic scattering at very low momentum transfers. The second DSSD (hereafter DSSD#2) is located at 32.5° with respect to the beam axis at a distance of 354 mm from IR. The main aim of deploying this DSSD is to measure the α particles originating from the Isoscaler Giant Monopole Resonance (ISGMR) and (Isoscaler Giant Dipole Resonanse) ISGDR processes.

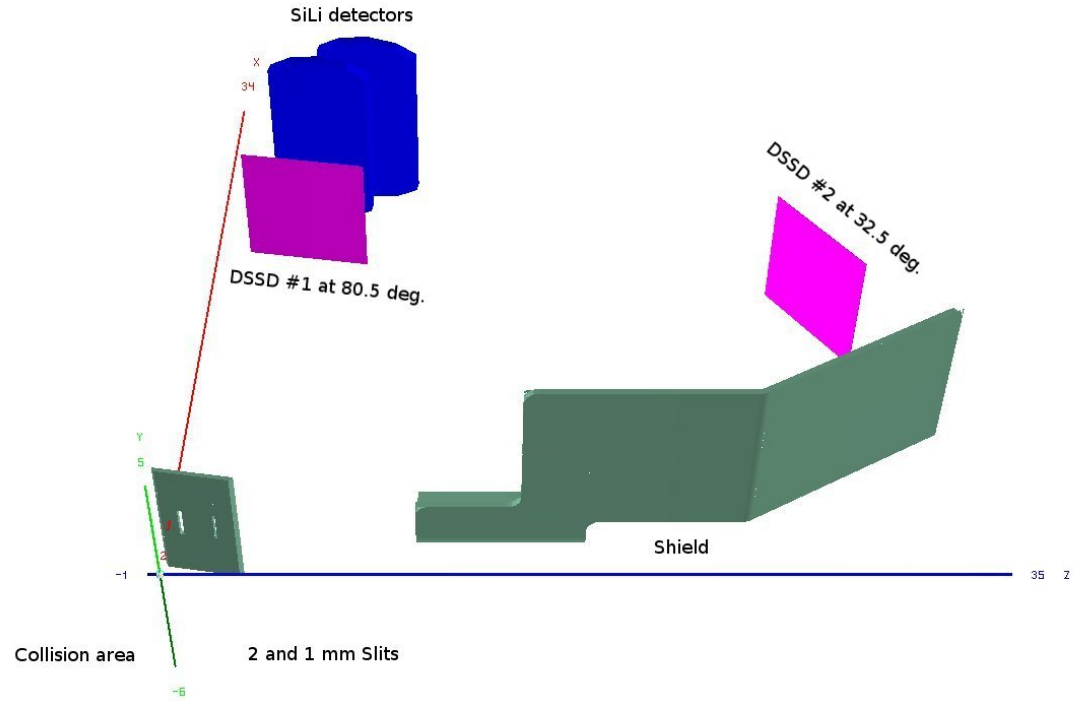

Figure 3: Target-chamber components, including two DSSDs, Slit, Shield, and two SiLi detectors. The z-axis represents the direction of the beam. The center of the coordinate system is the same as the interaction point.

2.2 SiLi

Behind DSSD#1 one there are two 6.5 mm thick Lithium-drifted Silicon detectors (SiLi) to measure the energy of fast light ejectiles punching through DSSD#1. Each SiLi has an effective area of around 54×102 mm^2, as the detectors have round corners.

2.3 Slit

Since the gas jet target has presumably a guassian shape profile density in x and y directions, with a sigma of about 4 mm, and the beam has also a width of 1 mm, therefore, the interaction

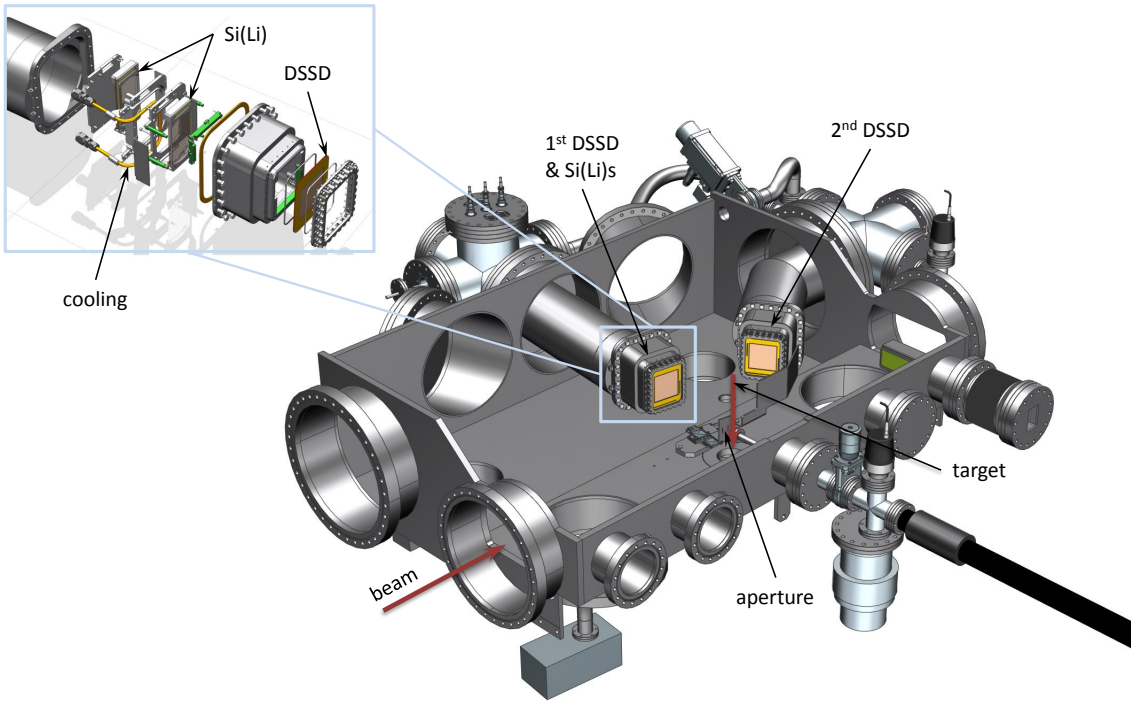

Figure 4: Schematic drawing of the target chamber.

profile is far from being point like. This, of course, leads to a low angular resolution. In order to improve the angular resolution at the cost of the luminosity an object made of tantalum, which has two vertical rectangular-shaped windows, was put between the interaction area and the DSSD#1. This object, so-called the slit, is 59.2 mm long, 32.0 mm wide, and 2 mm thick. The width of the rectangular windows are 1 and 2 mm. Furthermore, they are 1.5 cm apart.

2.4 Shield

Shield, as shown in figure 3, is meant to stop the light ions scattered at 90° along the beam trajectory from reaching DSSD#2. In fact, the residual gas coming from the gas jet target may scatter off the high velocity circulating beam and bombard DSSD#2. Although, the density of the residual gas is very small, it is compensated by the Rutherford cross sections at 90° which is huge. This would lead to low-energy background on DSSD#2.

2.5 Pin Diode

Pin diode detectors are six square-shaped silicon detectors with an area of 10×10 mm^2 and thickness of 0.5 mm, see figure 5. The pins are put on a substrate forming a table with three rows and two columns. The substrate is positioned perpendicular to the beam direction, facing

the beam. The transversal position of the pins is controllable. The distance between the sides of the pin-diodes, both vertically and horizontally, is 2 mm. The pins are almost 8 meters downstream from the IR which is after the quadrupole doublet and before the dipole. The pins are employed in this experiment to detect ^{58}Ni and/or ^{56}Ni scattered off H_2 or ^{4}He target. There is also a chance to detect the decay fragments coming out of the excited ^{58}Ni* and/or ^{56}Ni*.

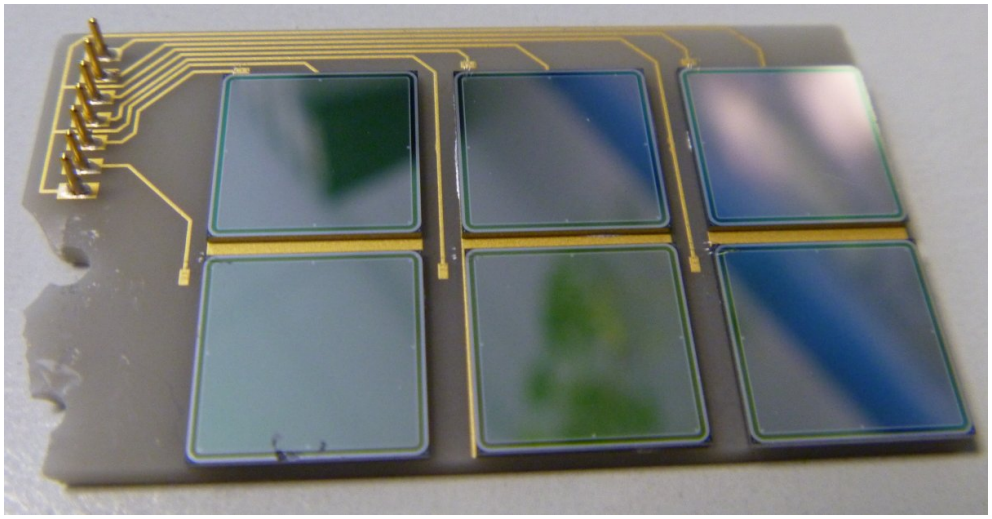

Figure 5: The array of pin diodes on the substrate.

2.6 Quadrupoles

As mentioned before, the pin diodes were placed after a doublet of quadrupoles. Therefore, the beam-like particles and the fragment elements which might be detected by the pin diodes, first go through the doublet of quadruploes, before they are detected. As a result, they are affected by the magnetic field of the quadrupoles.

Implementation of magnetic fields in the simulation could be done in two ways. Either, the magnetic field maps have to be implemented directly, or the transfer matrices of each element must be used. In fact, using transfer matrices is preferred. They are more easily accessible, and the simulation would be done with less CPU cycles. However, the problem is that Geant4 toolkit is not designed to interpret the transfer matrices. In order to use the transfer matrices in the simulation, a class was added to simulation intervening in the stepping action at the level of `G4UserSteppingAction` [4]. The procedure is as follows: once the charged particle enters the magnetic element, its position and momentum vectors are obtained. Then by applying the transfer matrix on them, the momentum and position vectors of the particle while exiting the element are calculated. At this level, `G4Stepping` methods accessible to user are utilized to apply the new momentum and position of the particle.

One should note that though the usage of the transfer matrices reduces the CPU time, but it has a main drawback. Using this technique, all possible physical processes that the particle might have undergone while flying through the magnetic element are ignored.

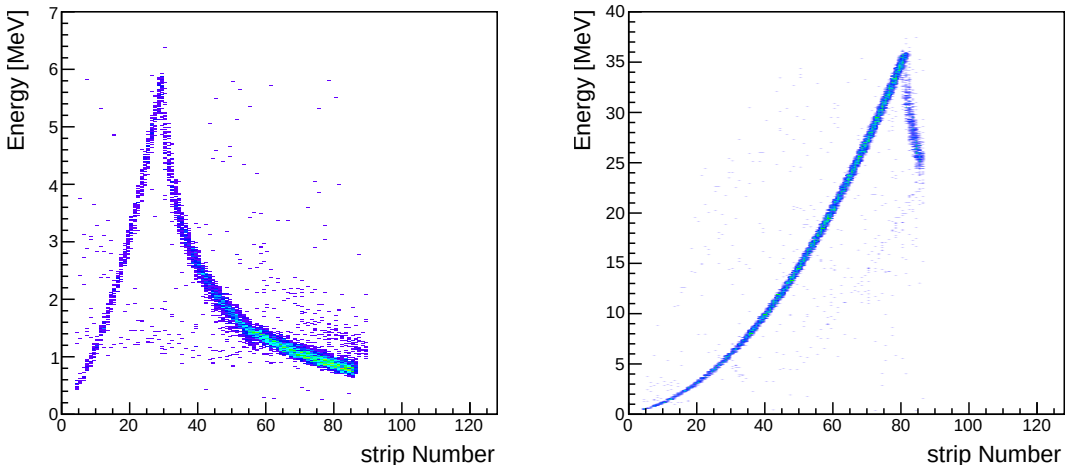

Figure 6: Left panel (right panel), energy deposited on DSSD#1 (energy deposited on DSSD#1 plus energy deposited on SiLi1) by protons as a function of strip number. The beam was 150 MeV/u ^{58}Ni bombarding hydrogen target.

3 Results

Here, the response of the detectors to the reactions of interest are presented. Results given here are obtained using the `genbod` [5] event generator as the primary event generator. Please note that the genbod produces events based on phase space distribution. Unless mentioned, for all results presented here the slit is positioned 3 cm away from IR. In addition, the 1 mm wide slit is used.

3.1 DSSD and SiLi spectra

The first process to study is the elastic scattering of ^{56}Ni and ^{58}Ni beam with an incident energy of 400 MeV/u off hydrogen gas jet target. The cross sections for this reaction particularly at low momentum transfer regime could be used to probe nuclear matter density distribution. In figure 6 (left panel), the energy deposited on DSSD#1 as a function of DSSD strip number is shown. As illustrated, protons with energies less than ∼6 MeV are stopped in DSSD#1. However, protons with higher energies punch through the DSSD and reach the first SiLi detector located right behind the DSSD. In the right panel of the same figure the sum of the energy deposited on DSSD#1 and the SiLi is shown. Ascending band (in the left panel) represent protons stopped in the DSSD. Protons with energies above 6 MeV punch through the 0.285 mm thick DSSD, represented by the descending band in the same plot. On the right panel the total energy deposited on the DSSD#1 and the SiLi behind it is shown. As one can see, protons with energies above 35 MeV punch through the SiLi detector, as well.

Since the DSSD data are read through strip numbers it is needed to convert the strip number to scattering angle of the light target-like particles which reach the DSSD. The other question which needs to be addressed is the effect of inaccuracy in the determination of the transversal position of the slit on the scattering angle. However, ideally the IP and the center of the slit and the center of DSSD#1 are designed to be positioned on a straight line. In figure 7, left panel, the scattering angle of proton at the level of generation has been plotted as a function of

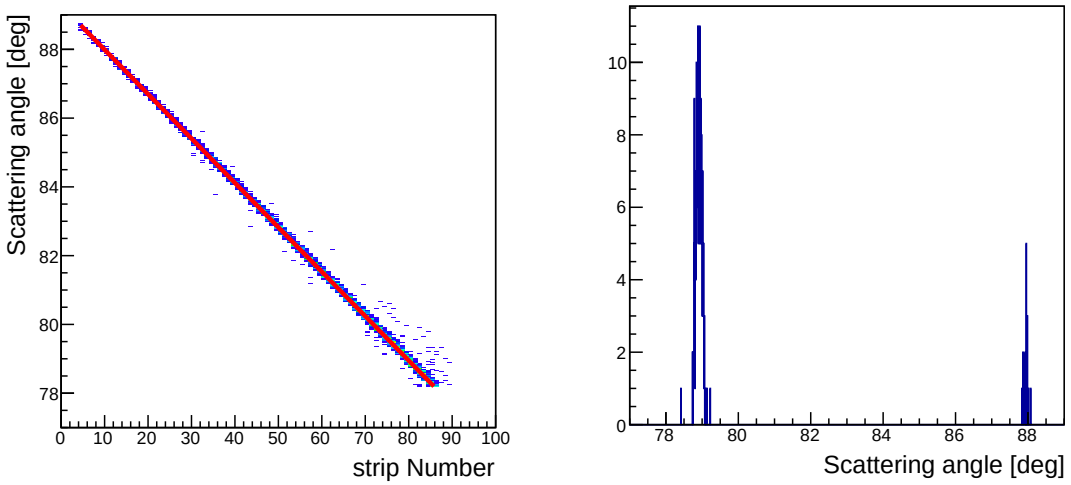

Figure 7: Left panel: scattering angle of protons as a function of the strip number, the red line is a straight line fitted through the band. Right panel: projection of the left panel spectrum on y-axis at strip numbers of 10 and 80. The width of the peaks is an indication of the systematic error in determination of the scattering angle which is almost 0.1° and 0.2°, respectively.

the strip number. The red straight line which has been fitted through the band is a first order polynomial, $y = -0.13x + 89.3$. Obviously, the band is thick and has a varying width, pointing to a systematic error in the conversion which depends on the scattering angle. In the right panel of the same figure, the widths of the band at the position of strip number 10 and 80 have been depicted. At strip number 10 and 80 the systematic error on the conversion from strip number to the scattering angle is almost 0.1° and 0.2°, respectively.

During the experiment care is taken to make sure that the center of the slit is located on a straight line connecting the center of DSSD#1 and the IP. However, there could be some deviation from that. In order to study the magnitude of that effect on the inaccuracy of the scattering angle, a simulation was performed with a slit 2 mm away from its original position. In figure 8, the energy spectra of DSSD#1 for both cases when the slit is in its right position (left band) and when its is off by 2 mm (right band) are shown. The 2 mm shift has led to a shift of the position of the punch through point, indicated by the red vertical lines, by 5 strips. Since 5 strips are equal to 0.6°, it is fair to say that for each millimeter there will be 0.3° inaccuracy in the scattering angle measurement.

To study ISGMR and ISGDR in ^{58}Ni and ^{56}Ni, beams of these two species with energies of 100 and 150 MeV/u were impinged on ^{4}He gas jet target. Colliding ^{58}Ni and ^{56}Ni with ^{4}He, there is always a possibility to excite the nucleus to its first 2^+ state. This state is above the ground state level by 1.45 MeV (2.7 MeV) for ^{58}Ni (^{56}Ni). In order to check the resolving power of the setup to distinguish between the α' and elastically scattered α, a series of simulations with 150 MeV/u and 100 MeV/u ^{58}Ni and ^{56}Ni beams on ^{4}He were performed. Here, only the results for 150 MeV/u beam energy are presented. On the left panel (right panel) of figure 9 the separation of the elastic band, left band, from the band relevant to ^{58}Ni (^{56}Ni) 2^+ state, right band, is clearly visible. As one can see in the picture the α with an energy above 24 MeV punches through the DSSD. In figure 10 (simulation) and in figure 11 (experimental data) the separation of 2^+ state from the elastic band for ^{58}Ni for two beam energies of 150 and 100 MeV/u, left

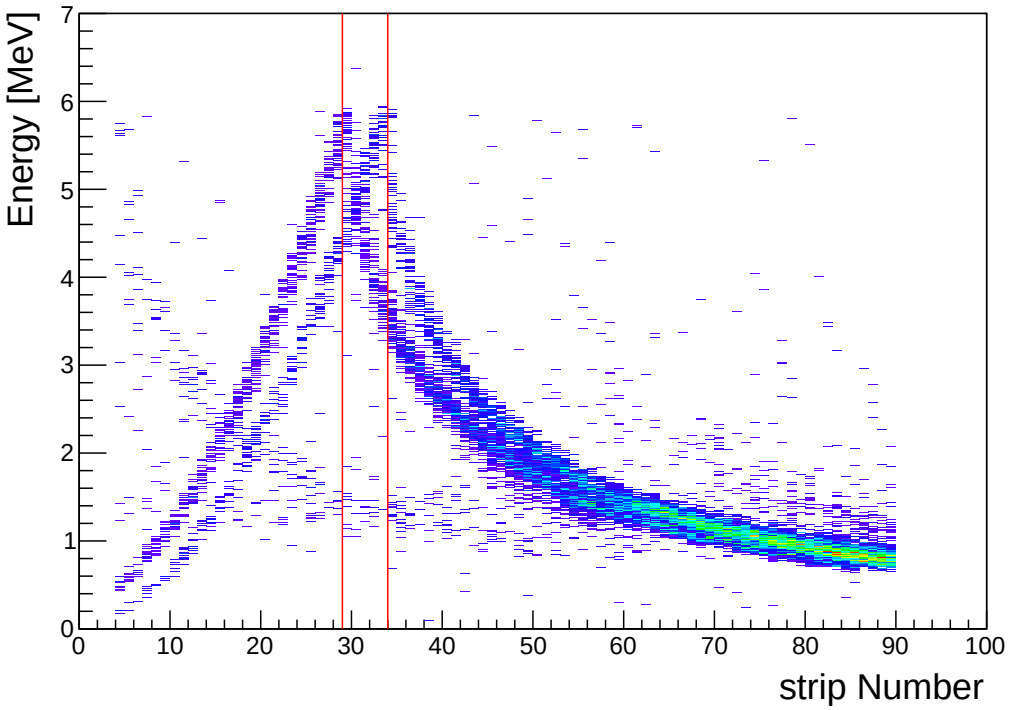

Figure 8: Energy spectra of DSSD#1 as a function of the strip number for two cases when the slit is placed at its original position, left band, compared to the case when the slit is 2 mm off, right band. The red vertical lines show the position of the punch-through point.

and right panels, are shown. Please note in these two figures the x-axis represents the scattering angle of the α' in lab.

3.2 Pin Diode spectra

The other detector used in the simulation was pin diode. As mentioned in the introduction, the pin diodes are located almost 8 meters downstream the IP after the quadrupole doublets. The pin diodes are placed inside the perimeter ring while the light-ion detectors are outside the ring, see figure 2. This way there will be the possibility to detect the heavy ions in coincidence with the light ejectiles detected by the DSSDs. Once ^{56}Ni or ^{58}Ni hit helium target, it is likely that Ni is excited to ISGMR. The excited nucleus decays right after the excitation into fragments. For instance ^{58}Ni may decay to ^{57}Ni and a neutron or, ^{57}Co and a proton. There is also the possibility for the excited ^{58}Ni to decay to ^{54}Fe and an α. Since the decay happens while the nucleus is traveling with a high velocity (100 or 150 MeV/u beam energy), in the laboratory frame, the decay fragments form a cone with a very small opening angle. In figure 12, the results for energy deposited by fast heavy fragments on the pin diodes for beam energy of 150 MeV/u ^{58}Ni are shown. As seen, the energy deposited by different fragments form a sort of structure. This phenomena is in qualitive agreement with what was observed in real data, figure 13. Though, the simulation is incapable of explinaining the experimenal observation quantitively. This is not a surpprise, as it is well known that Geant4 has serious shortcoming in predicting energy

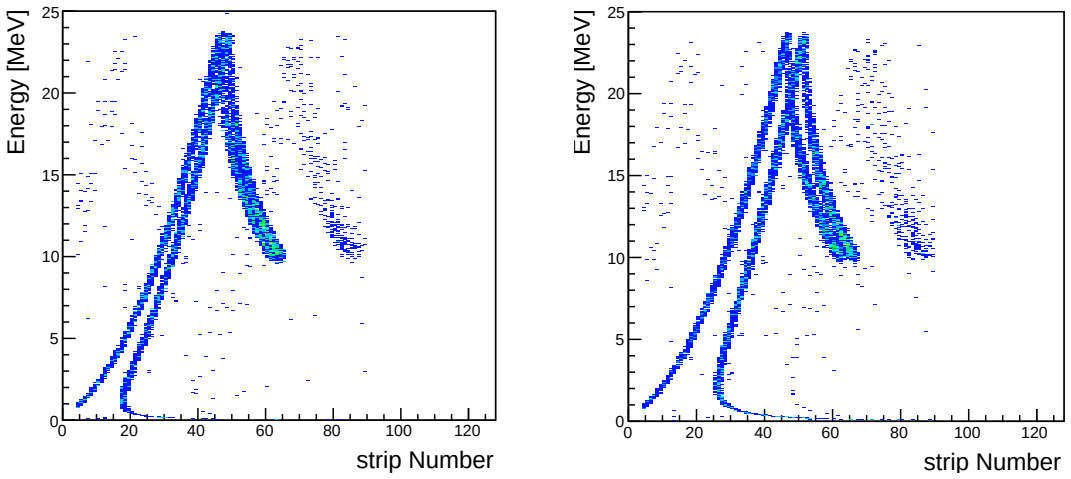

Figure 9: Left panel (right panel): clear separation of the elastic band, left band, from the 2^+ state, right band, for 150 MeV/u ^{58}Ni (^{56}Ni) beam.

deposition by heavy ions.

The projection of the decay cone containing the decay product, namely ^{54}Fe on transversal plane at the place of the pin diodes is shown in figure 14. More specifically, to generate this decay fragment the fragment generator was set to take ^{58}Ni (150 MeV/u) as incoming beam impinging on ^{4}He target. Furthermore, the ^{58}Ni is excited to ISGMR state, and α' is required to be detected by DSSD#2. Then the generator is set for the decay ^{58}Ni* to ^{54}Fe and α on-the-fly. The opening angle of the cone turns out to be less than 0.8°. The cone is originally symmetric in both transversal directions (x and y), but after passing through the quadrupoles it takes the shape of an ellipse, as shown in figure 14. As seen in this figure the major axis of the density ellipse is twice as big as its minor axis. In this picture the pin diodes are shown by six squares in yellow color. The top panel shows the pin diode when it is at its closest distance to the beam, 6 mm. For this case the total coincidence acceptance which is the percentage of the ^{54}Fe detected by the pins while their α' counter-part is detected by DSSD#2 is around 1.47%. However, when the pins are put on the edge of the cone, at the kinematic turning point, the coincidence acceptance increases to 3.04%.

A clear message from this simulation is that the coincidence acceptance is very small. However, in order to measure ISGMR and ISGDR reactions it is certainly needed to cut the background utilizing the coincidence technique. The urgent need to improve on the coincidence acceptance led to an extensive study to obtain an optimal position for the pin diode detector along the beam pipe as well as an optimal configuration for them. That study revealed that there is no unique and comprehensive optimized location for the pins; optimizing for a particular decay fragment, beam energy or excitation energy would lead to the loss of acceptance for another fragment and/or excitation energies.

The coincidence acceptance could be increased up to 50% by approaching the cone from both sides of the beam while covering the cone with as many pin diodes as possible. Such a test was done for the 293 cm location downstream of the IP which is already accessible from both sides with 44 pins covering as much of the phase space as possible; see figure 15. In this figure, it is seen that the cone has been shifted to the right. This has to do with the fact that the α' was

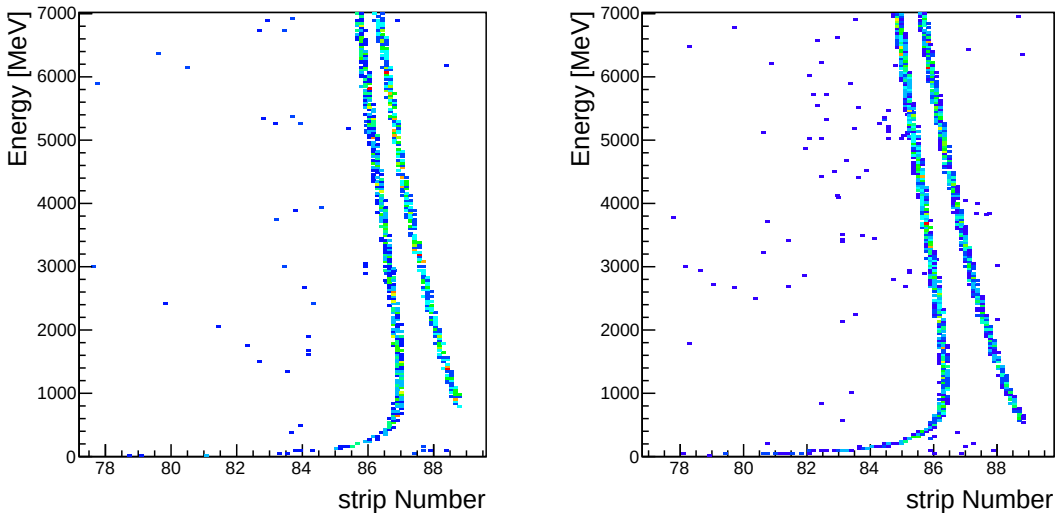

Figure 10: Simulation, left panel (right panel) showing the clear separation of the elastic band, left band, from the 2^+ state, right band, for ^{58}Ni for beam energy of 150 MeV/u (100 MeV/u). The x axis represents the scattering angle in the laboratory

required to be detected by DSSD#2 which is placed on the left side of the beam. Therefore, ^{52}Fe receives a recoil to the right.

4 Summary

Here, a short report of examples of simulations for fast ejectiles and heavy-ion detectors is presented. For this work, experiment E105 at the GSI ESR was chosen, which is a prototype experiment for EXL. The simulation was done using Geant4 toolkit. The same simulation was performed within FairROOT framework through which one may use Geant4, Geant3, or Fluka as the simulation engine. The simulation was unique in the sense that instead of using magnetic maps to mimic the effect of magnetic fields on the charged particles transfer matrices were used.

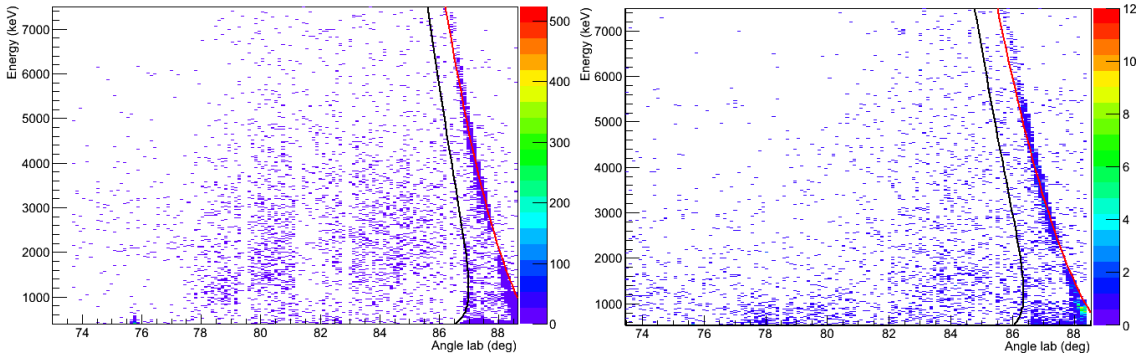

Figure 11: Same as figure 10 but for experimental data.

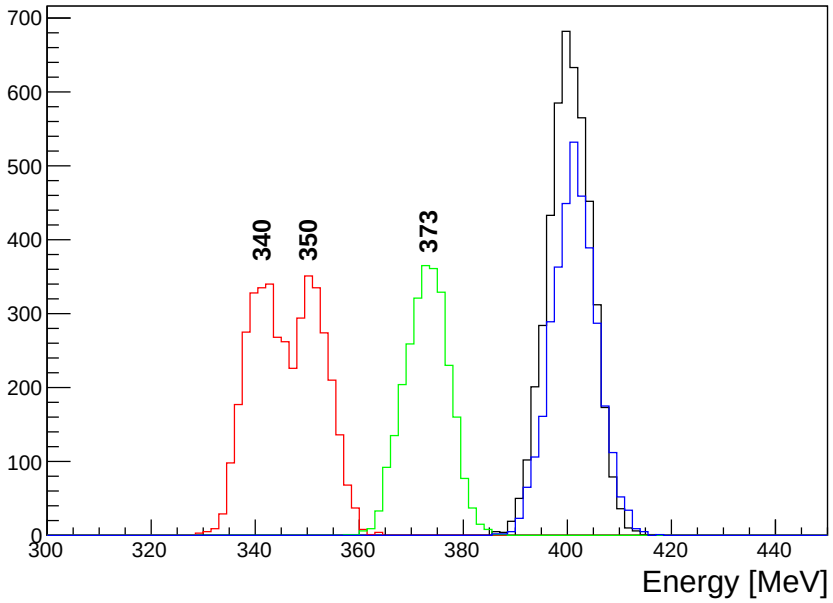

Figure 12: Simulation for energy deposition by ^{57}Ni (blue), ^{57}Co (green), ^{54}Fe (red) which are decay fragmets of ^{58}Ni* for ^{58}Ni beam with an energy of 150 MeV/u. The black line represent the energy deposited by ^{58}Ni elastically scattered.

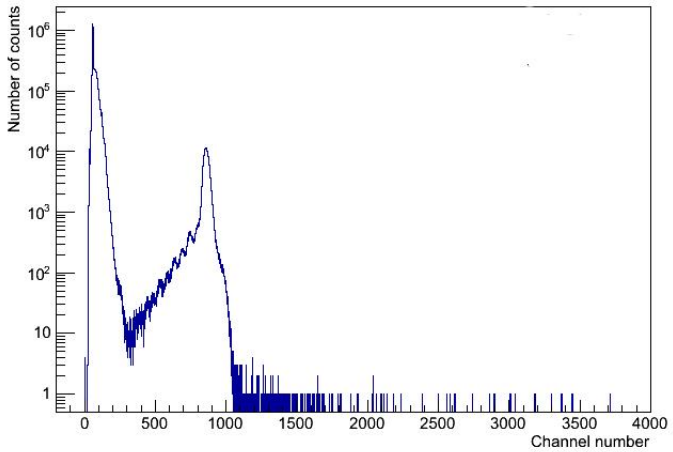

Figure 13: ADC channel number of the pin diode, for ^{58}Ni beam with a beam energy of 150 MeV/u. Please note that the spectrum is not calibrated.

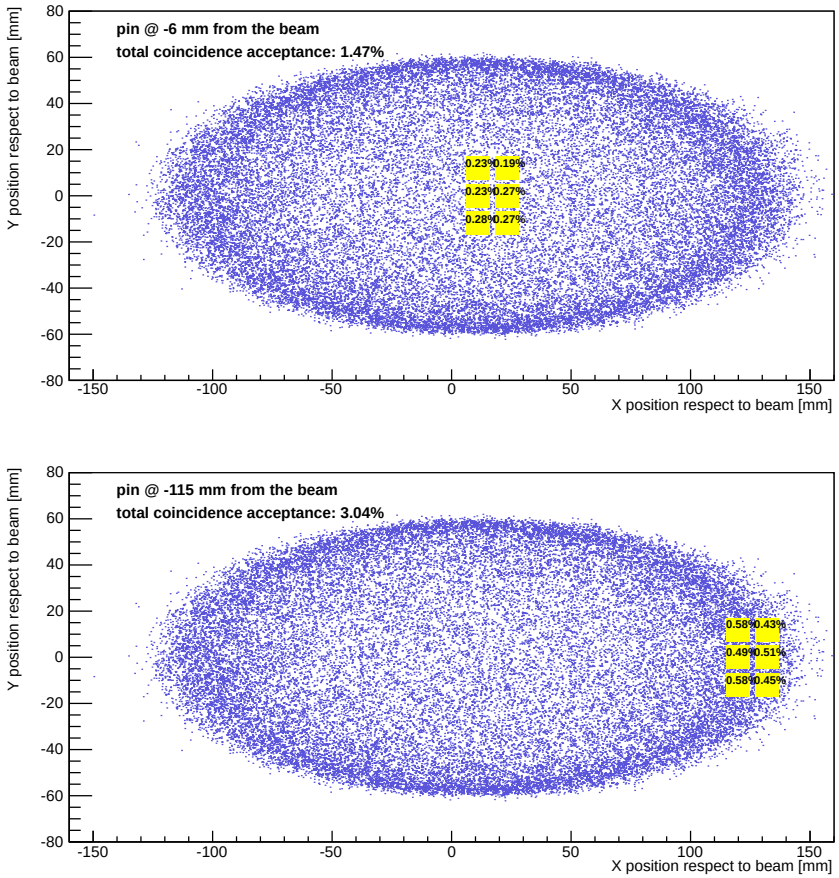

Figure 14: Transversal distribution of ^{54}Fe decay fragment 8 meters away from the target position, after the doublet quadrupole. Total coincidence acceptance is 1.47% (3.04%) when pins are placed 6 mm (115 mm) away from the beam orbit, top panel (bottom panel). The numbers on each pin shows the coincidence acceptance for that particular pin.

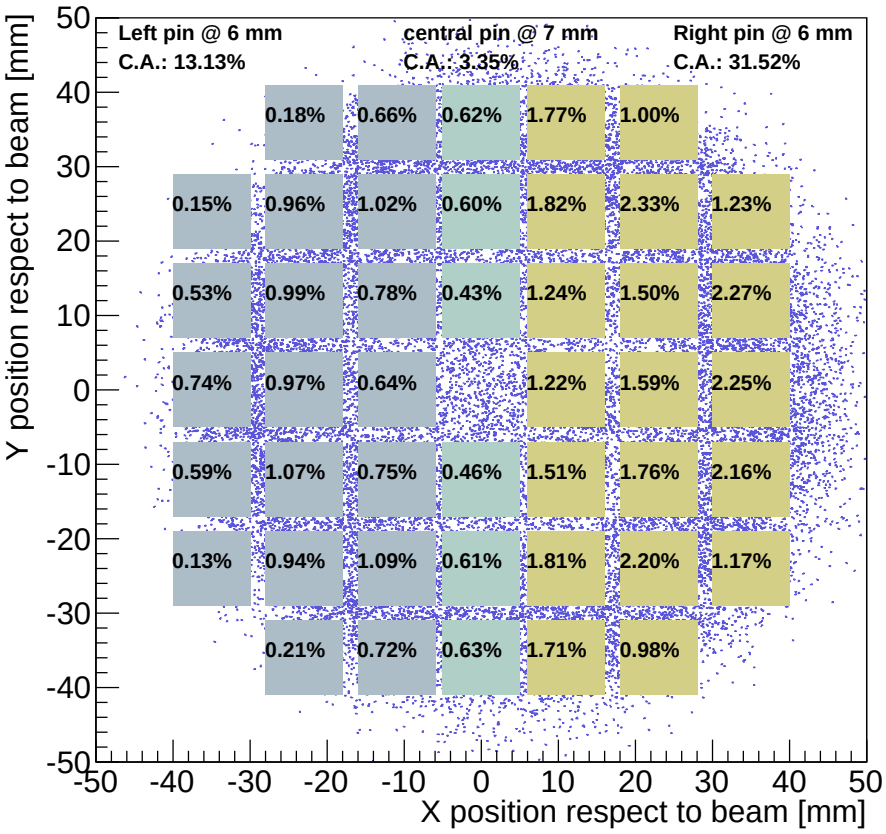

Figure 15: Distribution of ^{52}Fe decay fragment at 2.93 m downstream from the target, approaching the beam from both side. The numbers indicated on each pin are the coincidence acceptance of that pin. C.A. stands for coincidence acceptance. The 6 mm, 7 mm and 6 mm written on the top of the figure show the closest distance of the left, middle, and right set of pins to the center of the beam.

More specifically, a class was developed which intervenes in the process of stepping action through `G4UserSteppingAction`. It should be noted that this is presently possible only for Geant4. In order to use transfer matrices in the FairROOT framework further code development from the community in charge is required.

In addition, a decay-fragment event generator was developed. The generator is capable of generating any kind of two-body decays on-the-fly. However, in this simulation it was just used to study the decay of ISGMR and ISGDR excited states of ^{58}Ni and ^{56}Ni. While using Geant4, the generator is used in integrated form. However, a stand-alone form of the generator was also developed which produces events in ASCII format readable to R3BAsciiGenerator class. For doing simulation in the FairROOT one may use the stand-alone version.

5 Recommendations

Adding transfer matrices to Geant4 and FairROOT through the base code is recommended. In fact, what we did was to intervene in the stepping action which is accessible to the user. The effect of magnetic field could be implemented by introducing that effect as a process in the base code.

The possibility to implement magnetic maps both in Geant4 and FairROOT exist. In addition, in Geant4, it is already possible to introduce dipoles and quadrupoles, directly. First steps in this direction (introducing dipoles and quadrupoles directly) in FairROOT are being taken within PandaROOT framework. It is recommended that such an implementation is also done in FairBase in a way that everybody can use it. Furthermore, it would be desirable if both Geant4 and FairROOT could interpret sextupoles as well.

In analyzing the E105 experimental data, it was found that the α' coming out of ISGMR reactions would be overshadowed by low-energy background and noise. This signals the urgent need for detecting the heavy fragments in coincidence with the α'. The current simulation showed how one may obtain a coincidence acceptance of almost 50% by putting a number of pin diodes in the right place (see the text) and increase the spatial coverage of the fragments.

Apart from recommendations given above which were concluded based on the simulations reported here, it is also very much recommended to improve the Geant4 heavy ion physics packages (Geant3 is no longer developed). The shortcomings of Geant4 and Geant3 in the prediction of the energy deposition by reletivistic heavy ions are well known. This is an essential part for the simulation of the NuSTAR (Nuclear Structure, Astrophysics and Reactions) experiments planned to be performed at FAIR (Facility for Antiproton and Ion Research in Europe) in the coming years.

References

[1] N. Kalantar *et al.* Approved GSI PAC proposal E105, Start up of part of the EXL physics program with ^{56}Ni.

[2] S. Agostinelli *et al.* Nucl. Instr. Meth. Phys. Res. A 506, 250 (2003).

[3] M. Al-Turany *et al.* J. Phys. Conf. Ser. 396, 022001 (2012).

[4] M. Mahjour-Shafiei, N. Kalantar-Nayestanaki, and H. Weick, Chinese J. Phys. 48, 560 (2010).

[5] F. James, Monte Carlo Phase Space, CERN 68-15 (1968).